

Relativistic Plasma Polarizer: Impact of Temperature Anisotropy on Relativistic Transparency

David J. Stark,^{1,2} Chinmoy Bhattacharjee,^{1,2} Alexey V. Arefiev,² Toma Toncian,³ R. D. Hazeltine,^{1,2} and S. M. Mahajan^{1,2,4}

¹*Department of Physics, The University of Texas at Austin, Texas 78712, USA*

²*Institute for Fusion Studies, The University of Texas at Austin, Texas 78712, USA*

³*Center for High Energy Density Science, The University of Texas at Austin, Texas 78712, USA*

⁴*Shiv Nadar University, NH91, Tehsil Dadri, Gautam Buddha Nagar, Uttar Pradesh 201 314, India*

(Received 13 July 2014; revised manuscript received 4 December 2014; published 8 July 2015)

3D particle-in-cell simulations demonstrate that the enhanced transparency of a relativistically hot plasma is sensitive to how the energy is partitioned between different degrees of freedom. For an anisotropic electron distribution, propagation characteristics, like the critical density, will depend on the polarization of the electromagnetic wave. Despite the onset of the Weibel instability in such plasmas, the anisotropy can persist long enough to affect laser propagation. This plasma can then function as a polarizer or a wave plate to dramatically alter the pulse polarization.

DOI: 10.1103/PhysRevLett.115.025002

PACS numbers: 52.27.Ny, 52.35.Hr, 52.38.-r, 52.65.-y

When the electron population in a plasma reaches relativistic energies, the dielectric properties can change drastically enough for the plasma to become transparent to an electromagnetic (EM) wave that cannot penetrate a low-energy plasma of the same density. When the electrons are brought to these energies directly by the electromagnetic pulse (of high intensity), the resulting phenomenon is called self-induced transparency [1]. The enhanced transparency, however, is an intrinsic characteristic of a relativistically hot plasma independent of the source of heating. In the era of high-power lasers, when experimental studies of relativistic plasmas are possible for a staggering variety of applications (proton therapy, material studies, laboratory astrophysics, basic dynamics), a detailed understanding of relativistic transparency will be essential, both for a proper interpretation of experiments and as a new diagnostic tool. Earlier theoretical studies of self-induced transparency dealt with high amplitude wave solutions in homogeneous and weakly inhomogeneous plasmas [2–6]. Most recently, progress has been made in understanding the plasma-wave interaction at the plasma-vacuum interface and the onset of relativistic transparency as a high intensity pulse irradiates a cold plasma slab [7–14].

In most studies on the subject, focused on determining how the transparency threshold scales with both the plasma density and the intensity of the irradiating pulse, the pulse serves the dual purpose of imparting relativistic energy to electrons and simultaneously acting as a probe of criticality. These experiments, concentrating on the total electron energy, do not fully investigate the role that the shape of the electron distribution could play in determining the transparency threshold. The approach is consistent with the commonly used explanation that the relativistic mass increase, by lowering the plasma frequency, raises the critical density below which the electromagnetic waves are

able to propagate. Since the relativistic γ factor is a gross measure of the overall energy, this explanation could not reveal if the propagation characteristics are affected by the way the energy is partitioned between different degrees of freedom. Because the critical density for electromagnetic waves in warm nonrelativistic plasmas is independent of the shape of the electron distribution, a similar conclusion in the relativistic case may appear to be justifiable; most experiments are designed and interpreted within this context.

However, one could envision an alternative system setup in which a plasma is heated to relativistic temperatures by a high-power pump pulse and then probed with a low-amplitude pulse, allowing the properties of the created distribution function to be tested without changing the distribution itself. Indeed, several experiments have used a transverse optical pulse to probe the system during the laser-plasma interaction [15–18]. Characterizing relativistic transparency's effects on pulse propagation enables the probe to serve as a diagnostic for the plasma energy, temperature, and especially anisotropy. This information, in turn, is crucial to the interpretation and prediction of the high-amplitude pulse's behavior in the plasma. The better characterization of a laser-produced distribution has particular relevance to laboratory astrophysics [19,20] and ion acceleration from laser-irradiated solid-density targets [21–26].

In this Letter we demonstrate that relativistic transparency is strongly affected by how the electron energy is partitioned between different degrees of freedom. We consider here the simplest problem: the propagation of a low amplitude pulse through a preformed relativistically hot anisotropic electron plasma (ion motion is neglected) to explore its intrinsic dielectric properties (unchanged by the weak pulse). We find that (1) the critical density for propagation depends strongly on the pulse polarization, (2) two plasmas with the same density and average energy

per electron can exhibit profoundly different responses to electromagnetic pulses, and (3) the anisotropy-driven Weibel instability develops as expected; the time scales of the growth and backreaction (on anisotropy), however, are long enough that sufficient anisotropy persists for the entire duration of the simulation, consequently impacting the optical properties. Modified propagation characteristics add a qualitative new element in developing a more advanced understanding of laser-plasma interactions. Relativistic thermal plasmas with electron anisotropy can naturally arise in laser-irradiated targets. For ultrathin targets, the heating is volumetric [1,27,28], whereas for thick targets the heating occurs at the front surface of the target and the hot plasma is produced as a result of target expansion at the rear side [26,28–30], where a persistent double layer separates the cold electrons from the expanding plasma [31]. In both cases, temperature anisotropy in their electron populations is observed [25,29,32]; the most direct support comes from 3D particle-in-cell (PIC) simulations in the thick-target regime that show the hot electron distribution in the expanding plasma [28].

Using a 3D-3V particle-in-cell simulation (three spatial and three velocity dimensions), we study the dynamics of a low amplitude circularly polarized electromagnetic pulse incident on a finite slab of constant density electrons (ions fixed) with an anisotropic relativistic temperature. The domain is $130 \times 70 \times 70 \mu\text{m}$ ($4500 \times 100 \times 100$ cells) and consists of vacuum regions at $-30 \mu\text{m} < x < 0$ and $8 \mu\text{m} < x < 100 \mu\text{m}$ and a plasma region at $0 < x < 8 \mu\text{m}$. A circularly polarized Gaussian pulse [full width half maximum (FWHM) of 50 fs] of wavelength $\lambda = 2 \mu\text{m}$ [33] enters the plasma from negative x and focuses halfway into the target with intensity FWHM of $11.8 \mu\text{m}$. The pulse has focal amplitude of $a = |e|E_0/m_e c \omega = 0.2$, where E_0 is the electric field amplitude, ω is the wave frequency, c is the speed of light, and m_e and e are the electron mass and charge, respectively. The electron number density n ramps up and falls off as a semi-Gaussian of FWHM $2.5 \mu\text{m}$, so that $n = 2.7n_*$ for $2.3 \mu\text{m} < x < 5.7 \mu\text{m}$. Here $n_* \equiv m_e \omega^2 / 4\pi e^2$ is the classical critical density. We use 120 electrons per cell to initialize an anisotropic momentum distribution given by

$$f_0 = \frac{n}{I(\alpha, \epsilon)} \exp\left(-\alpha \sqrt{1 + \frac{p_z^2 + (1-\epsilon)(p_x^2 + p_y^2)}{m_e^2 c^2}}\right), \quad (1)$$

where $1/\alpha$ is an effective temperature normalized to $m_e c^2$ and ϵ introduces anisotropy into the distribution (when $\epsilon \neq 0$). In Eq. (1), n is the electron density, p is the electron momentum, and I is a dimensionless normalization constant

$$I(\alpha, \epsilon) = \int \exp\left(-\alpha \sqrt{1 + \frac{p_z^2 + (1-\epsilon)(p_x^2 + p_y^2)}{m_e^2 c^2}}\right) \frac{d^3 p}{(m_e c)^3}. \quad (2)$$

For $\epsilon > 0$, the motion along the z axis is always associated with less energy than in the other directions. In the simulation

we use $\alpha = 2.0$ and $\epsilon = 0.45$, corresponding with average particle energy $\langle E \rangle = 1.24 \text{ MeV}$, and $\sqrt{\langle p_y^2 \rangle / \langle p_z^2 \rangle} = 1.35$. Here the brackets represent an average over the entire momentum space so that $\langle R \rangle \equiv \int R f_0 d^3 p / (m_e c)^3$.

The simulation begins ($t = 0$) with the leading edge of the circularly polarized pulse at $x = 0$. In Fig. 1, the transmitted and reflected pulses are shown 140 fs into the simulation. The pink surfaces denote surfaces of constant $E^2 = 8.0 \times 10^{22} \text{ (V/m)}^2$, whereas the images on the bottom and side of the box represent E_y and E_z at $z = 0$. The ion number density is also projected onto the bottom and side of the box to show where the plasma resides. The simulation results are quite spectacular: the plasma acts as a powerful polarizer; it reflects almost all of the parallel component (to the axis of anisotropy z), $E_z \equiv E_{\parallel}$, while it transmits much of the perpendicularly polarized component, $E_y \equiv E_{\perp}$. The latter hotter direction is favored for propagation [36].

Since an anisotropic electron distribution is subject to the Weibel instability [37], we have carefully monitored the growth of energy stored in the magnetic field of the system ($\int B^2 / 8\pi dV$). We have displayed in Fig. 1 both the magnetic energy and $\sqrt{\langle p_y^2 \rangle / \langle p_z^2 \rangle}$ as functions of the simulation time. Note that $\sqrt{\langle p_y^2 \rangle / \langle p_z^2 \rangle}$ starts slightly below the analytically predicted value of 1.35 at $t = 0$, a discrepancy of order 2%.

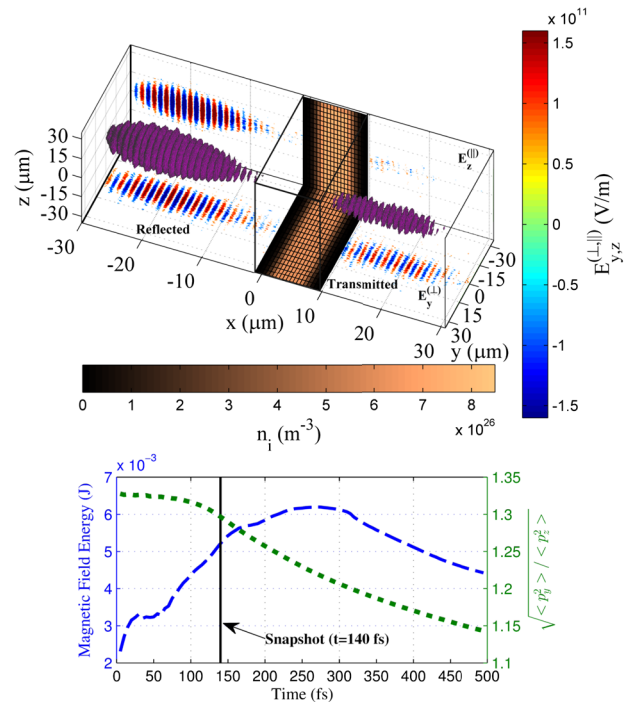


FIG. 1 (color online). Surfaces of constant intensity of the reflected and transmitted pulses 140 fs after the pulse hits the target (top panel). E_y and E_z cross sections at $z = 0$ are given on the bottom and side of the box, respectively, along with n_i . The magnetic field energy and $\sqrt{\langle p_y^2 \rangle / \langle p_z^2 \rangle}$ are plotted throughout the simulation time (bottom panel).

This can be improved by increasing the sampling resolution of the distribution function (shrinking the p_x , p_y , and p_z step size). Recent work has shown kinetic simulations of the relativistic Weibel instability from thermal anisotropy [38,39], which also exhibit, similar to our results, a peak in magnetic field energy right before falling to an asymptotic value. Here we observe that the anisotropy persists in the plasma over a sufficiently long time scale to be probed. The pulse has already passed through the plasma well before $\sqrt{\langle p_y^2 \rangle / \langle p_z^2 \rangle}$ has appreciably diminished.

We next calculate, analytically, the critical frequency and density for the plasma distribution invoked in the simulation [see Eq. (1)]. A simple linear analysis for wave propagation will demonstrate the disparity in critical densities based on polarization. Some examples of earlier studies of anisotropic plasmas are [40–42]. The basic dynamics is contained in the covariant Vlasov and Maxwell's equations (the momentum four-vector p^μ is normalized to m_e , and $c = 1$):

$$\left[p^\mu \partial_\mu + q p_\nu F^{\mu\nu} \frac{\partial}{\partial p^\mu} \right] f(x, p) = 0, \quad (3)$$

$$\partial_\mu F^{\mu\nu} = 4\pi J^\nu, \quad (4)$$

where $f(x, p)$ is the electron distribution function, $J^\nu = q/m \int d^4 p p^\nu f(x, p)$ is the four-current, and $F^{\mu\nu} = \partial^\mu A^\nu - \partial^\nu A^\mu$ is the electromagnetic field tensor, A^μ being the potential four-vector. The summation convention is used, with metric $(+, -, -, -)$. We linearize Eqs. (3) and (4), and assume perturbations of the form $f_1, F_1, A_1 \propto \exp(-ik_\mu x^\mu)$, choosing $k^\mu = (\omega, k, 0, 0)$. In a field-free plasma, and for the equilibrium distribution given by Eq. (1), the two transverse modes A_1^y and A_1^z are decoupled, each producing current only parallel to its respective polarization. From these independent dispersion relations, the expression of the critical frequency for each mode is derived by setting $k = 0$ and solving for ω :

$$\omega_{(\perp, \parallel)}^2 = \frac{\alpha(1-\epsilon)^{(1,0)} \omega_{p0}^2}{I(\alpha, \epsilon)} \times \int d^3 p \frac{p_{(y,z)}^2 \exp\left(-\alpha \sqrt{1+p_z^2 + (1-\epsilon)(p_x^2 + p_y^2)}\right)}{\sqrt{1+p^2} \sqrt{1+p_z^2 + (1-\epsilon)(p_x^2 + p_y^2)}}, \quad (5)$$

where $\omega_{p0} \equiv \sqrt{4\pi n e^2 / m_e}$ is the plasma frequency. The subscripts \perp (\parallel) for the modes with nonzero A_y (A_z) indicate the direction of the electric field in relation to the axis of anisotropy. One can readily find the critical densities for each mode directly from Eq. (5): $n_{(\perp, \parallel)} = (\omega_{p0} / \omega_{(\perp, \parallel)})^2 n_*$, again with $n_* \equiv m_e \omega^2 / 4\pi e^2$.

The expressions for ω_\perp and ω_\parallel become more tractable in the case of weak anisotropy, i.e., for $\epsilon \ll 1$. To the leading order,

$$\omega_{(\perp, \parallel)}^2 = \frac{\alpha^2 \omega_{p0}^2}{K_2(\alpha)} \left[\int_\alpha^\infty dz \frac{K_2(z)}{z^2} - (2, 1)\epsilon G(\alpha) \right], \quad (6)$$

$$G(\alpha) = \int_\alpha^\infty dz \frac{K_2(z)}{z^2} + \frac{1}{2} \int_\alpha^\infty dz \left(\frac{\alpha^2}{z^3} - \frac{1}{z} \right) K_3(z), \quad (7)$$

where K_i is the modified Bessel function of the second kind of order i . For the isotropic distribution ($\epsilon = 0$), naturally $n_\perp = n_\parallel$. Notice that $n_\perp > n_\parallel$ for $\epsilon > 0$; the critical density is lower for a wave whose electric field is polarized along the axis of anisotropy, that is, the colder direction in this simulation. This result is consistent with the presented simulation, where the density was $n = 2.70n_*$. For the simulation's laser frequency, $n_\perp = 2.74n_*$ and $n_\parallel = 2.50n_*$, so that only the y component should pass through. Figure 2 shows how the disparity in critical densities between the two polarizations, calculated from Eq. (5), increases both with ϵ and effective temperature $1/\alpha$. The solid lines indicate the contours of constant $\langle E \rangle$, and the ratio n_\perp/n_\parallel changes considerably along these contours; the relativistic transparency varies rapidly with temperature anisotropy even when the average energy is kept constant.

Qualitatively, the effect can be understood by considering a single electron whose momentum \mathbf{p}_0 changes by $\delta\mathbf{p}$ due to the interaction with the laser field. The corresponding change in the electron velocity is $\delta\mathbf{v} = [\gamma^2 \delta\mathbf{p} - \mathbf{p}_0(\mathbf{p}_0 \cdot \delta\mathbf{p})] / \gamma^3$, where $\gamma = \sqrt{1 + p_0^2}$ and all momenta are normalized to $m_e c$. This change and the resulting electron current is smaller by a factor γ^2 for $\delta\mathbf{p} \parallel \mathbf{p}_0$ than for $\delta\mathbf{p} \perp \mathbf{p}_0$. Thus, the plasma will be more transparent for the electric field polarized along the hotter direction, because this field will induce a smaller electron current.

The anisotropy-induced discrepancy in the critical densities has a profound effect on wave propagation; this is true even when the plasma is transparent (low density) to arbitrary polarization. For demonstration, we conduct a 3D-3V simulation, complementary to the earlier one, in which a linearly polarized Gaussian pulse is incident on a finite

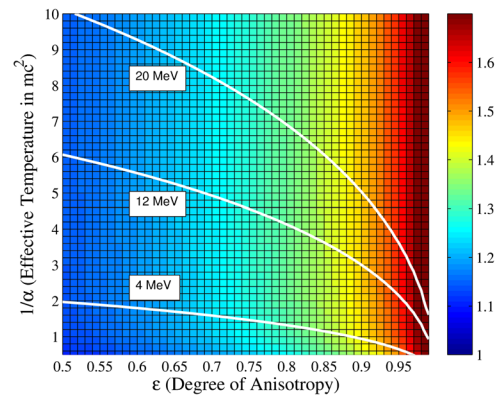


FIG. 2 (color online). Ratio of critical densities, n_\perp/n_\parallel , as a function of effective electron temperature $1/\alpha$ and the degree of anisotropy ϵ . The solid lines indicate the contours of constant average electron energy.

length subcritical plasma with an anisotropic distribution. A less energetic electron distribution is used [$\alpha = 8.0$, $\epsilon = 0.45$, $n_{\parallel} = 1.38$, $n_{\perp} = 1.46$, $\langle E \rangle = 0.67$ MeV; represented in (p_y, p_z) space in the inset of Fig. 3] to demonstrate that even more moderate energies can still exhibit this pronounced effect, and now the density $n = 1.05n_*$ is chosen so that both $n < n_{\perp}$ and $n < n_{\parallel}$. The pulse is polarized at a 45° angle to the axis of anisotropy, so that $E_y = E_z$ in the incoming pulse. The pulse width has FWHM 50 fs, peak $a = 0.14$, $\lambda = 1.0 \mu\text{m}$, and intensity FWHM $11.8 \mu\text{m}$. The simulation domain now consists of a vacuum region at $x < 0$ and a plasma region at $0 \leq x \leq 12 \mu\text{m}$. The density ramps up and falls off as a semi-Gaussian of FWHM $0.7 \mu\text{m}$, so that $n = 1.05n_*$ for $1.1 \mu\text{m} < x < 10.9 \mu\text{m}$.

The incoming pulse can be decomposed into two modes: one polarized along the axis of anisotropy and the other perpendicular to it. These modes are decoupled and have two different critical densities. For a cold plasma, the phase velocity $v_p = \omega/k = (1 - n/n_*)^{-1/2}$ is determined by the critical density n_* . By analogy, due to the difference between n_{\parallel} and n_{\perp} , we expect a considerable discrepancy in phase velocities between the two modes, particularly because the density is close to critical. In Fig. 3, following the pulse before (black) and after (red) it passes through the plasma, we see that the induced phase separation of the two modes changes the pulse from linear to elliptical polarization, highlighting the expected discrepancy in v_p ; in this scenario the plasma serves as a wave plate. Both of our simulations demonstrate how a relativistic plasma can change the polarization of an electromagnetic wave; naturally the excess (shortage) of the wave angular momentum is compensated by the corresponding loss (gain) by the plasma.

Figure 3 clearly demonstrates that anisotropy-induced polarization change is essentially a relativistic phenomenon.

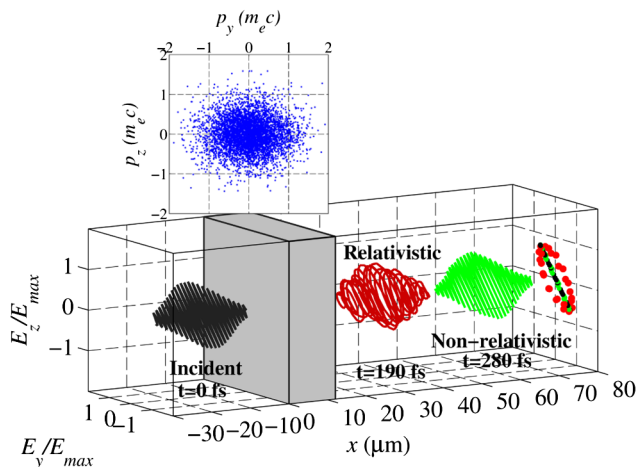


FIG. 3 (color online). Plots of the incident pulse (at $t = 0$), the transmitted pulse through the relativistic plasma (at $t = 190$ fs, $\alpha = 8.0$, and $\epsilon = 0.45$), and the transmitted pulse through the nonrelativistic plasma (at $t = 280$ fs, $\alpha = 500$, and $\epsilon = 0.45$) are denoted in black, red, and green, respectively. The inset represents the relativistic distribution function in (p_y, p_z) space.

In a nonrelativistic anisotropic plasma the phase velocity depends on the polarization, but the critical density does not. Consequently, the linear polarization of the wave remains essentially unaffected after the initial pulse (black) propagates through the plasma (green). The parameters for the nonrelativistic simulation are $\alpha = 500$ and $\epsilon = 0.45$ with an average kinetic energy ≈ 0.002 MeV, much smaller than the rest mass energy. We also set $n = 0.75n_*$ to ensure that both polarizations penetrate the plasma and reduce the amplitude to $a = 0.07$. The relativistic anisotropic plasma, in stark contrast, changes the linear polarization to elliptical.

An investigation of the interaction of electromagnetic waves with relativistically anisotropic plasmas, thus, reveals a new qualitative phenomenon: the propagation characteristics (critical density, effective refractive index) of the wave are controlled not only by plasma density and average electron energy but also by how the energy is partitioned between different degrees of freedom, i.e., by anisotropy. An anisotropic plasma emerges as an effective polarizer; it will filter out the electric field of the pulse polarized in the “colder” direction, and pulses of the same frequency, polarized in the hot direction, will be preferentially transmitted. Even if the plasma is transparent for all polarizations, the discrepancy in the critical densities causes phase separation of the modes, manifested as an altered polarization of the pulse so that the plasma here serves as a wave plate.

Besides facilitating the examination of the plasmas generated in the thin and thick target laser-plasma systems, our results are relevant for interpreting the data from probe pulses simultaneously incident on the plasma with the pump pulse. Polarization shifts in the probe pulse over time serve as a measure of the temperature anisotropy evolution. Such shifts could, in fact, compete with Faraday rotation of the probe pulse used in magnetic field measurements [43]. One could also envision utilizing anisotropic plasma as the basis for new optical devices used for beam polarization or polarization smoothing [44–47]. Differential propagation characteristics can even affect high-harmonic and synchrotron transmission through dense laser-irradiated targets [48,49].

Finally, the findings of this paper, in particular the impact of temperature anisotropy on relativistic transparency, can potentially play a pivotal role in understanding phenomena in high-energy astrophysics. It is well known, for example, that compressive shocks in jets and relativistic flows [associated with active galactic nuclei and gamma-ray bursts (GRBs)] can heat plasmas to relativistic temperatures [53–50]]. Any anisotropy in the shock heating could affect the radiation traversing this hot medium. In particular, the forward and reverse shocks typically associated with the optical and radio afterglows of GRBs could be prime candidates for exhibiting anisotropy-induced polarization shifts [54]. Polarization dependences observed in the optical afterglows [55–58] are usually attributed to magnetic fields, but thermal anisotropy could also be a major contributing factor. These astrophysical systems along with high-power laser-plasma experiments are best suited

to showcase differential propagation, as the effects are expected to be spectacular for high temperature plasmas.

Simulations were performed using EPOCH code (developed under UK EPSRC Grants No. EP/G054940/1, No. EP/G055165/1, and No. EP/G056803/1) using HPC resources provided by the TACC at the University of Texas. We acknowledge valuable discussions with Amir Shahmoradi and Patrick Crumley. This work was supported by the U.S. DOE Contract No. DE-FG02-04ER54742, NNSA Contract No. DE-FC52-08NA28512, and DOE SCGF administered by ORISE-ORAU under Contract No. DE-AC05-06OR23100 (D. J. S.).

-
- [1] S. Palaniyappan *et al.*, *Nat. Phys.* **8**, 763 (2012).
 [2] A. I. Akhiezer and R. V. Polovin, *Sov. Phys. JETP* **3**, 696 (1956).
 [3] P. Kaw and J. Dawson, *Phys. Fluids* **13**, 472 (1970).
 [4] C. Max and F. Perkins, *Phys. Rev. Lett.* **27**, 1342 (1971).
 [5] J. H. Marburger and R. F. Trooper, *Phys. Rev. Lett.* **35**, 1001 (1975).
 [6] C. S. Lai, *Phys. Rev. Lett.* **36**, 966 (1976).
 [7] V. I. Eremin, A. V. Korzhimanov, and A. V. Kim, *Phys. Plasmas* **17**, 043102 (2010).
 [8] F. Cattani, A. Kim, D. Anderson, and M. Lisak, *Phys. Rev. E* **62**, 1234 (2000).
 [9] V. V. Goloviznin and T. J. Schep, *Phys. Plasmas* **7**, 1564 (2000).
 [10] E. Siminos, M. Grech, S. Skupin, T. Schlegel, and V. T. Tikhonchuk, *Phys. Rev. E* **86**, 056404 (2012).
 [11] S. V. Bulanov, T. Zh. Esirkepov, M. Kando, S. S. Bulanov, S. G. Rykovanov, and F. Pegoraro, *Phys. Plasmas* **20**, 123114 (2013).
 [12] S. M. Weng, M. Murakami, P. Mulser, and Z. M. Sheng, *New J. Phys.* **14**, 063026 (2012).
 [13] V. A. Vshikov, N. M. Naumova, F. Pegoraro, and S. V. Bulanov, *Phys. Plasmas* **5**, 2727 (1998).
 [14] M. Tushentsov, A. Kim, F. Cattani, D. Anderson, and M. Lisak, *Phys. Rev. Lett.* **87**, 275002 (2001).
 [15] A. Buck, M. Nicolai, K. Schmid, C. M. S. Sears, A. Sävert, J. M. Mikhailova, F. Krausz, M. C. Kaluza, and L. Veisz, *Nat. Phys.* **7**, 543 (2011).
 [16] M. B. Schwab *et al.*, *Appl. Phys. Lett.* **103**, 191118 (2013).
 [17] O. Jäckel, J. Polz, S. M. Pfoth, H.-P. Schlenvoigt, H. Schwoerer, and M. C. Kaluza, *New J. Phys.* **12**, 103027 (2010).
 [18] M. C. Kaluza, H.-P. Schlenvoigt, S. P. D. Mangles, A. G. R. Thomas, A. E. Dangor, H. Schwoerer, W. B. Mori, Z. Najmudin, and K. M. Krushelnick, *Phys. Rev. Lett.* **105**, 115002 (2010).
 [19] S. V. Bulanov, T. Zh. Esirkepov, D. Habs, F. Pegoraro, and T. Tajima, *Eur. Phys. J. D* **55**, 483 (2009).
 [20] T. Zh. Esirkepov and S. V. Bulanov, *EAS Publication Series* **58**, 7 (2012).
 [21] O. Shorokhov and A. Pukhov, *Laser Particle Beams* **22**, 175 (2004).
 [22] L. Yin, B. J. Albright, D. Jung, R. C. Shah, S. Palaniyappan, K. J. Bowers, A. Henig, J. C. Fernandez, and B. M. Hegelich, *Phys. Plasmas* **18**, 063103 (2011).
 [23] A. A. Sahai, F. S. Tsung, A. R. Tableman, W. B. Mori, and T. C. Katsouleas, *Phys. Rev. E* **88**, 043105 (2013).
 [24] A. Macchi, M. Borghesi, and M. Passoni, *Rev. Mod. Phys.* **85**, 751 (2013).
 [25] B. M. Hegelich *et al.*, *New J. Phys.* **15**, 085015 (2013).
 [26] M. Schollmeier *et al.*, *Phys. Plasmas* **22**, 043116 (2015).
 [27] L. Yin, B. J. Albright, D. Jung, R. C. Shah, S. Palaniyappan, K. J. Bowers, A. Henig, J. C. Fernández, and B. M. Hegelich, *Phys. Plasmas* **18**, 063103 (2011).
 [28] J.-L. Liu, M. Chen, J. Zheng, Z.-M. Sheng, and C.-S. Liu, *Phys. Plasmas* **20**, 063107 (2013).
 [29] K. Zeil, J. Metzkes, T. Kluge, M. Bussmann, T. E. Cowan, S. D. Kraft, R. Sauerbrey, and U. Schramm, *Nat. Commun.* **3**, 874 (2012).
 [30] T. Kluge, T. Cowan, A. Debus, U. Schramm, K. Zeil, and M. Bussmann, *Phys. Rev. Lett.* **107**, 205003 (2011).
 [31] B. N. Breizman, A. V. Arefiev, and M. V. Fomyts'kyi, *Phys. Plasmas* **12**, 056706 (2005).
 [32] L. Yin, B. J. Albright, K. J. Bowers, D. Jung, J. C. Fernández, and B. M. Hegelich, *Phys. Rev. Lett.* **107**, 045003 (2011).
 [33] A 2 μm laser can be generated using techniques discussed in Refs. [34] and [35].
 [34] K. Scholle, S. Lamrini, P. Koopmann, and P. Fuhrberg, in *Frontiers in Guided Wave Optics and Optoelectronics*, edited by B. Pal (InTech, Croatia, 2010), Chap. 21 [<http://cdn.intechopen.com/pdfs-wm/8446.pdf>].
 [35] P. Wan, L.-M. Yang, and J. Liu, *Opt. Express* **21**, 1798 (2013).
 [36] See Supplemental Material at <http://link.aps.org/supplemental/10.1103/PhysRevLett.115.025002> for a video of the simulation shown in Fig. 1.
 [37] E. W. Weibel, *Phys. Rev. Lett.* **2**, 83 (1959).
 [38] H. H. Kaang, C.-M. Ryu, and P. H. Yoon, *Phys. Plasmas* **16**, 082103 (2009).
 [39] A. Ghizzo, *Phys. Plasmas* **20**, 082111 (2013).
 [40] R. Schlickeiser, *Phys. Plasmas* **11**, 5532 (2004).
 [41] U. Schaefer-Rolffs and R. Schlickeiser, *Phys. Plasmas* **12**, 022104 (2005).
 [42] M. Lazar and R. Schlickeiser, *Phys. Plasmas* **13**, 012110 (2006).
 [43] M. Roth, *J. Instrum.* **6**, R09001 (2011).
 [44] P. Michel, L. Divol, D. Turnbull, and J. D. Moody, *Phys. Rev. Lett.* **113**, 205001 (2014).
 [45] E. Lefebvre, R. L. Berger, A. B. Langdon, B. J. MacGowan, J. E. Rothenberg, and E. A. Williams, *Phys. Plasmas* **5**, 2701 (1998).
 [46] D. H. Munro, S. H. Dixit, A. B. Langdon, and J. R. Murray, *Appl. Opt.* **43**, 6639 (2004).
 [47] J. E. Rothenberg, *J. Appl. Phys.* **87**, 3654 (2000).
 [48] R. Horlein *et al.*, *Laser Particle Beams* **29**, 383 (2011).
 [49] B. Dromey *et al.*, *Nat. Phys.* **8**, 804 (2012).
 [50] L. Sironi and A. Spitkovsky, *Astrophys. J.* **726**, 75 (2011).
 [51] L. Sironi and A. Spitkovsky, *Astrophys. J.* **698**, 1523 (2009).
 [52] A. Spitkovsky, *Astrophys. J.*, **673**, L39 (2008).
 [53] A. Spitkovsky, *AIP Conf. Proc.* **801**, 345 (2005).
 [54] P. Kumar and B. Zhang, *Phys. Rep.* **561**, 1 (2015).
 [55] I. A. Steele, C. G. Mundell, R. J. Smith, S. Kobayashi, and C. Guidorzi, *Nature (London)* **462**, 767 (2009).
 [56] J. Greiner *et al.*, *Nature (London)* **426**, 157 (2003).
 [57] K. Wiersema *et al.*, *Nature (London)* **509**, 201 (2014).
 [58] C. G. Mundell *et al.*, *Nature (London)* **504**, 119 (2013).